

Dynamics of Bloch vector in thermal Jaynes-Cummings model

Hiroo Azuma*

2-1-12 MinamiFukunishi-cho, Oe, NishiKyo-ku,
Kyoto-shi, Kyoto 610-1113, Japan

November 26, 2018

Abstract

In this paper, we investigate the dynamics of the Bloch vector of a single two-level atom which interacts with a single quantized electromagnetic field mode according to the Jaynes-Cummings model, where the field is initially prepared in a thermal state. The time evolution of the Bloch vector $\mathbf{S}(t)$ seems to be in complete disorder because of the thermal distribution of the initial state of the field. Both the norm and the direction of $\mathbf{S}(t)$ oscillate hard and their periods seem infinite. We observe that the trajectory of the time evolution of $\mathbf{S}(t)$ in the two- or three-dimensional space does not form a closed path. To remove the fast frequency oscillation from the trajectory, we take the time-average of the Bloch vector $\mathbf{S}(t)$. We examine the histogram of $\{S_z(n\Delta t) | n = 0, 1, \dots, N\}$ for small Δt and large N . It represents an absolute value of a derivative of the inverse function of $S_z(t)$. (When the inverse function of $y = S_z(t)$ is a multi-valued function, the histogram represents a summation of the absolute values of its derivatives at points whose real parts are equal to y on the Riemann surface.) We examine the dependence of the variance of the histogram on the temperature of the field.

1 Introduction

The Jaynes-Cummings model (JCM) is a solvable quantum mechanical model of a single two-level atom in a single electromagnetic field mode [1, 2, 3, 4, 5]. This model is originally designed for studying a spontaneous emission. The interaction term is obtained by the rotating wave approximation. In this interaction, each photon creation causes an atomic de-excitation and each photon annihilation causes an atomic excitation.

If the photon number is sharply defined in the initial state of the field, the JCM shows the Rabi oscillations in the populations of the atomic levels. If the initial state of the

*On leave from Research Center for Quantum Information Science, Tamagawa University Research Institute, 6-1-1 Tamagawa-Gakuen, Machida-shi, Tokyo 194-8610, Japan, Electronic address: hiroo.azuma@m3.dion.ne.jp

field is a coherent state, the oscillation of the mean photon number collapses and revives in the JCM. In this way, the JCM reveals the quantum natures of the radiation.

Because the JCM is exactly solvable, it is investigated from various viewpoints. The JCM whose boson field is prepared in a thermal state is discussed in Refs. [6, 7]. Thermodynamics of the JCM is discussed in Ref. [8]. In this analysis, the grand partition function of both the atom and the boson field is considered. Extended JCMs are studied as dissipative models [9, 10]. Recently, the JCM has been used for describing the evolution of the entanglement between the atom and the field [11, 12]. In Refs. [11, 12], the electromagnetic field is assumed to be initially prepared in a thermal state.

In this paper, we consider the dynamics of the Bloch vector of a two-level atom interacting with a single mode boson according to the JCM, where the initial state of the boson is in thermal equilibrium. The time evolution of the Bloch vector $\mathbf{S}(t)$ seems to be in a state of complete disorder because of the thermal distribution of the initial state of the boson field. The trajectory of $\mathbf{S}(t)$ oscillates hard and seems to wander without a purpose. We try to find a property that characterizes this confused movement of $\mathbf{S}(t)$.

If $S_x(0) \neq 0$ or $S_y(0) \neq 0$, the time evolution of the Bloch vector $\mathbf{S}(t)$ draws a trajectory in the two- or three-dimensional space. We observe that this trajectory does not form a closed path. To remove the fast frequency oscillation from the trajectory, we take the time-average of the $\mathbf{S}(t)$ as $\langle \mathbf{S} \rangle = \lim_{T \rightarrow \infty} (1/T) \int_0^T dt \mathbf{S}(t)$. We find that $\langle S_x \rangle$ and $\langle S_y \rangle$ are equal to zero $\forall \beta, \omega$ and ω_0 , where β is an inverse of the temperature for the initial thermal state of the field, ω is an angular frequency of the field and $\hbar\omega_0$ is an energy gap of the two-level atom. $\langle S_z \rangle$ takes a certain function of β, ω and ω_0 .

We take the histogram of samples $\{S_z(n\Delta t) | n = 0, 1, \dots, N\}$ for small Δt and large N . We understand that it represents an absolute value of a derivative of the inverse function of $S_z(t)$. (When the inverse function of $y = S_z(t)$ is a multi-valued function, the histogram represents a summation of the absolute values of its derivatives $|(d/dy)S_z^{-1}|$ at points whose real parts are equal to y on the Riemann surface.) We approximate obtained histograms in the high temperature by the probability function of the normal distribution. We examine the dependence of the variance of the samples on the temperature β .

This paper is organized as follows: In Sec. 2, we derive an equation which governs the time evolution of the Bloch vector $\mathbf{S}(t)$. In Sec. 3, we examine the trajectory of $\mathbf{S}(t)$ and observe that it does not form a closed path. In Sec. 4, we take the time-average of $\mathbf{S}(t)$ for the case where the field is resonant with the atom. In Sec. 5, we take the histogram of data of $S_z(t)$ sampled at intervals of Δt . In Sec. 6, we take the time-average of $\mathbf{S}(t)$ for the non-resonant case. In Sec. 7, we give brief discussions.

2 The time evolution of the Bloch vector

In this section, we give the equation of the time evolution of the Bloch vector of the atom. The Jaynes-Cummings model is a system that is described by the following Hamiltonian:

$$H = \frac{\hbar}{2}\omega_0\sigma_z + \hbar\omega a^\dagger a + \hbar g(\sigma_+ a + \sigma_- a^\dagger), \quad (1)$$

where

$$\sigma_\pm = \frac{1}{2}(\sigma_x \pm i\sigma_y), \quad (2)$$

$$\sigma_x = \begin{pmatrix} 0 & 1 \\ 1 & 0 \end{pmatrix}, \quad \sigma_y = \begin{pmatrix} 0 & -i \\ i & 0 \end{pmatrix}, \quad \sigma_z = \begin{pmatrix} 1 & 0 \\ 0 & -1 \end{pmatrix}, \quad (3)$$

and $[a, a^\dagger] = 1$. The Pauli matrices ($\sigma_i, i = x, y, z$) are operators of the atom and a and a^\dagger are operators of the field. In this paper, we assume that g is a constant, so that it does not depend on ω_0 or ω . Let us divide H as follows [4, 5]:

$$H = \hbar(C_1 + C_2), \quad (4)$$

$$C_1 = \omega\left(\frac{1}{2}\sigma_z + a^\dagger a\right), \quad (5)$$

$$C_2 = g(\sigma_+ a + \sigma_- a^\dagger) - \frac{\Delta\omega}{2}\sigma_z, \quad (6)$$

where $\Delta\omega = \omega - \omega_0$. We can confirm

$$[C_1, C_2] = 0. \quad (7)$$

Because C_1 can be diagonalized at ease, we take the following interaction picture. We write a state vector of the whole system in the Schrödinger picture as $|\psi(t)\rangle$. A state vector in the interaction picture is defined by

$$|\psi_I(t)\rangle = \exp(iC_1 t)|\psi(t)\rangle. \quad (8)$$

(We assume $|\psi_I(0)\rangle = |\psi(0)\rangle$.) Because of Eq. (7), the time evolution of $|\psi_I(t)\rangle$ is given by

$$|\psi_I(t)\rangle = U(t)|\psi(0)\rangle, \quad (9)$$

where

$$U(t) = \exp(-iC_2 t). \quad (10)$$

We define the density operator of the initial state of the atom and the boson field as

$$\rho_{AF}(0) = \rho_A(0) \otimes \rho_F, \quad (11)$$

$$\rho_A(0) = \sum_{i,j \in \{0,1\}} \rho_{A,ij}(0) |i\rangle_{AA} \langle j|, \quad (12)$$

$$\rho_F = \frac{\exp(-\beta\hbar a^\dagger a)}{\text{Tr} \exp(-\beta\hbar a^\dagger a)} = (1 - e^{-\beta\hbar\omega}) \exp(-\beta\hbar a^\dagger a), \quad (13)$$

where

$$|0\rangle_A = \begin{pmatrix} 1 \\ 0 \end{pmatrix}, \quad |1\rangle_A = \begin{pmatrix} 0 \\ 1 \end{pmatrix}, \quad (14)$$

and β is an inverse of the temperature. (The indices A and F imply the atom and the field, respectively.)

The density operator of the atom in the interaction picture evolves according to

$$\rho_A(t) = \sum_{i,j \in \{0,1\}} \rho_{A,ij}(t) |i\rangle_{AA} \langle j|, \quad (15)$$

$$\rho_{A,ij}(t) = \sum_{k,l \in \{0,1\}} \rho_{A,kl}(0) A_{kl,ij}(t) \quad \text{for } i, j \in \{0,1\}, \quad (16)$$

$$A_{kl,ij}(t) = {}_A \langle i | \text{Tr}_F [U(t) (|k\rangle_{AA} \langle l| \otimes \rho_F) U^\dagger(t)] |j\rangle_A, \quad (17)$$

where Tr_F means a partial trace over the field. Because $\rho_{A,10}(t) = \rho_{A,01}(t)^*$ and $\rho_{A,11}(t) = 1 - \rho_{A,00}(t)$, we examine $\rho_{A,00}(t)$ and $\rho_{A,01}(t)$ only. We can derive $A_{kl,ij}(t)$ as follows: The unitary evolution operator of the whole system $U(t)$ given by Eqs. (6) and (10) is rewritten as

$$\begin{aligned} U(t) &= \exp[-it \begin{pmatrix} -\Delta\omega/2 & ga \\ ga^\dagger & \Delta\omega/2 \end{pmatrix}] \\ &= \sum_{n=0}^{\infty} \frac{(-1)^n t^{2n}}{(2n)!} \begin{pmatrix} (D+g^2)^n & 0 \\ 0 & D^n \end{pmatrix} \\ &\quad + \sum_{n=0}^{\infty} \frac{i(-1)^n t^{2n+1}}{(2n+1)!} \begin{pmatrix} -\Delta\omega(D+g^2)^n/2 & gaD^n \\ ga^\dagger(D+g^2)^n & \Delta\omega D^n/2 \end{pmatrix} \\ &= \begin{pmatrix} u_{00} & u_{01} \\ u_{10} & u_{11} \end{pmatrix}, \end{aligned} \quad (18)$$

where

$$D = \left(\frac{\Delta\omega}{2}\right)^2 + g^2 a^\dagger a, \quad (19)$$

$$\begin{aligned} u_{00} &= \cos(t\sqrt{D+g^2}) - \frac{i}{2}\Delta\omega \frac{\sin(t\sqrt{D+g^2})}{\sqrt{D+g^2}}, \\ u_{01} &= iga \frac{\sin(t\sqrt{D})}{\sqrt{D}}, \\ u_{10} &= iga^\dagger \frac{\sin(t\sqrt{D+g^2})}{\sqrt{D+g^2}}, \\ u_{11} &= \cos(t\sqrt{D}) + \frac{i}{2}\Delta\omega \frac{\sin(t\sqrt{D})}{\sqrt{D}}. \end{aligned} \quad (20)$$

(The trace over the field is taken by the basis vectors of the photon number states.) From Eqs. (17), (18), (19) and (20), we obtain

$$\begin{aligned} A_{00,00}(t) &= (1 - e^{-\beta\hbar\omega}) \sum_{n=0}^{\infty} \frac{(\Delta\omega/2)^2 + g^2(n+1) \cos^2(\sqrt{\tilde{D}(n+1)}t)}{\tilde{D}(n+1)} e^{-n\beta\hbar\omega}, \\ A_{11,00}(t) &= (1 - e^{-\beta\hbar\omega}) \sum_{n=1}^{\infty} g^2 n \frac{\sin^2(\sqrt{\tilde{D}(n)}t)}{\tilde{D}(n)} e^{-n\beta\hbar\omega}, \\ A_{01,01}(t) &= (1 - e^{-\beta\hbar\omega}) \sum_{n=0}^{\infty} \left[\cos(\sqrt{\tilde{D}(n+1)}t) - \frac{i}{2}\Delta\omega \frac{\sin(\sqrt{\tilde{D}(n+1)}t)}{\sqrt{\tilde{D}(n+1)}} \right] \\ &\quad \times \left[\cos(\sqrt{\tilde{D}(n)}t) - \frac{i}{2}\Delta\omega \frac{\sin(\sqrt{\tilde{D}(n)}t)}{\sqrt{\tilde{D}(n)}} \right] e^{-n\beta\hbar\omega}, \end{aligned} \quad (21)$$

$$A_{01,00}(t) = A_{10,00}(t) = A_{00,01}(t) = A_{10,01}(t) = A_{11,01}(t) = 0, \quad (22)$$

where

$$\tilde{D}(n) = \left(\frac{\Delta\omega}{2}\right)^2 + g^2 n. \quad (23)$$

We introduce the Bloch vector $\mathbf{S}(t) = (S_x(t), S_y(t), S_z(t))$ which is given by

$$\rho_A(t) = \frac{1}{2}(\mathbf{I} + \mathbf{S}(t) \cdot \boldsymbol{\sigma}), \quad (24)$$

where \mathbf{I} is the identity operator and $\boldsymbol{\sigma} = (\sigma_x, \sigma_y, \sigma_z)$. Because $\rho_A(t)^\dagger = \rho_A(t)$ and $\rho_A(t) \geq 0$, $\mathbf{S}(t)$ is a real vector and satisfies $|\mathbf{S}(t)|^2 \leq 1$. From Eqs. (16), (22) and (24), we obtain

$$\begin{aligned} \mathbf{S}(t) &= \mathcal{L}_{\Delta\omega}(t)\mathbf{S}(0) \\ &= \begin{pmatrix} L_{\Delta\omega}^{(1)}(t) & L_{\Delta\omega}^{(2)}(t) & 0 \\ -L_{\Delta\omega}^{(2)}(t) & L_{\Delta\omega}^{(1)}(t) & 0 \\ 0 & 0 & L_{\Delta\omega}^{(3)}(t) \end{pmatrix} \mathbf{S}(0) + \begin{pmatrix} 0 \\ 0 \\ L_{\Delta\omega}^{(4)}(t) \end{pmatrix}, \end{aligned} \quad (25)$$

where

$$\begin{aligned} L_{\Delta\omega}^{(1)}(t) &= \text{Re}[A_{01,01}(t)], \\ L_{\Delta\omega}^{(2)}(t) &= \text{Im}[A_{01,01}(t)], \\ L_{\Delta\omega}^{(3)}(t) &= A_{00,00}(t) - A_{11,00}(t), \\ L_{\Delta\omega}^{(4)}(t) &= A_{00,00}(t) + A_{11,00}(t) - 1. \end{aligned} \quad (26)$$

This is the equation of the time evolution of $\mathbf{S}(t)$.

3 The trajectory of the Bloch vector

In this section, we observe the trajectory of the time evolution of $\mathbf{S}(t)$. To simplify the discussion, we concentrate on the case where the field is resonant with the atom, that is, $\Delta\omega = 0$. Furthermore, we regard ω_0 as a constant. Thus, the model has two variables, t and β . We replace $|g|t$ with t and $\beta\hbar\omega$ ($=\beta\hbar\omega_0$) with β , where we assume $g \neq 0$ and $\omega_0 \neq 0$. They imply that the time t is in units of $|g|^{-1}$ and the inverse of the temperature β is in units of $(\hbar\omega_0)^{-1}$. From the above assumptions and Eqs. (21), (23), (25) and (26), we obtain the following equation:

$$\begin{aligned} \mathbf{S}(t) &= \mathcal{L}(t)\mathbf{S}(0) \\ &= \begin{pmatrix} L_1(t) & 0 & 0 \\ 0 & L_1(t) & 0 \\ 0 & 0 & L_3(t) \end{pmatrix} \mathbf{S}(0) + \begin{pmatrix} 0 \\ 0 \\ L_4(t) \end{pmatrix}, \end{aligned} \quad (27)$$

where

$$L_1(t) = (1 - e^{-\beta}) \sum_{n=0}^{\infty} \cos(\sqrt{n+1}t) \cos(\sqrt{n}t) e^{-n\beta}, \quad (28)$$

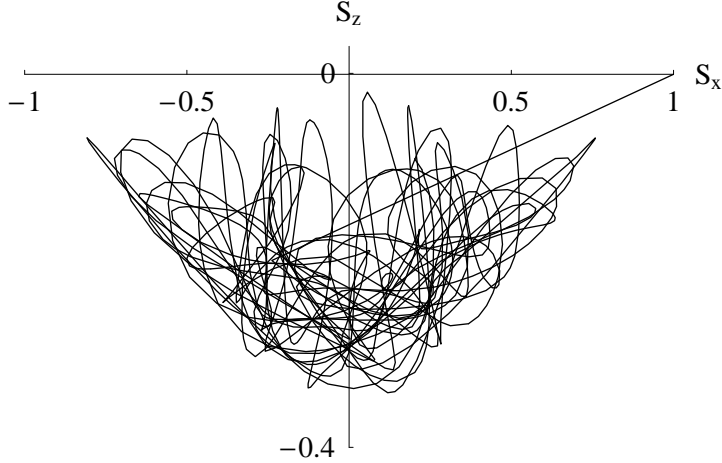


Figure 1: The trajectory of $\mathbf{S}(t)$ ($0 \leq t \leq 100$) whose initial state and temperature are given by $\mathbf{S}(0) = (1, 0, 0)$ and $\beta = 0.5$, respectively. (We assume $\Delta\omega = 0$.) The horizontal and vertical lines represent S_x and S_z , respectively. They are dimensionless quantities. In this case, the trajectory lies on the xz -plane. In the numerical calculation of $L_1(t)$ and $L_4(t)$ defined in Eqs. (28) and (30), the summations of the index n is carried out up to 500.

$$L_3(t) = \frac{1}{2}(1 - e^{-\beta}) + \frac{e^{2\beta} - 1}{2e^\beta} \sum_{n=1}^{\infty} \cos(2\sqrt{nt})e^{-n\beta}, \quad (29)$$

$$L_4(t) = -\frac{1}{2}(1 - e^{-\beta}) + \frac{(e^\beta - 1)^2}{2e^\beta} \sum_{n=1}^{\infty} \cos(2\sqrt{nt})e^{-n\beta}. \quad (30)$$

(We note $\text{Im}[A_{01,01}(t)] = 0$ for $\Delta\omega = 0$. In the algebraic form of $\text{Im}[A_{01,01}(t)]$, summations of $\cos(\sqrt{n+1}|g|t) \sin(\sqrt{n}|g|t)e^{-n\beta\hbar\omega}/\sqrt{n}$ and $\cos(\sqrt{n}|g|t) \sin(\sqrt{n+1}|g|t)e^{-n\beta\hbar\omega}/\sqrt{n+1}$ for the index n from 0 to ∞ appear, where $\sin(\sqrt{n}|g|t)/\sqrt{n}|_{n=0} = |g|t$. However, they converge to finite values. Similar discussions are explained in Sec. 4.) Looking at Eq. (27), we understand that the trajectory (a curve in the three-dimensional space of \mathbf{S} parameterized by t) is uniquely determined by the initial state $\mathbf{S}(0)$ for given β .

Figure 1 shows a trajectory of $\mathbf{S}(t)$ whose initial state and temperature are given by $\mathbf{S}(0) = (1, 0, 0)$ and $\beta = 0.5$, respectively. In this case, $S_y(t) = 0$ for $t \geq 0$ and the curve of $\mathbf{S}(t)$ lies on the xz -plane. The trajectory of Fig. 1 oscillates hard and seems to be in complete disorder. This is because $\mathbf{S}(t)$ is a tuple of superpositions of $\cos(\sqrt{n+1}t) \cos(\sqrt{n}t)e^{-n\beta}$ and $\cos(2\sqrt{nt})e^{-n\beta}$ for $n = 0, 1, 2, \dots$ as shown in Eqs. (28) and (30).

If the operator $\mathcal{L}(t)$ defined in Eq. (27) satisfies the relation $\mathcal{L}(t_2) = \mathcal{L}(t_2 - t_1)\mathcal{L}(t_1)$, the following thing can happen. If the trajectory reaches a point (at t_2) where it has passed before [at $t_1 (< t_2)$], it forms a closed path and $\mathbf{S}(t)$ moves along this closed path for $t \geq t_2$. (See Fig. 2.) However, this thing does not happen because $\mathcal{L}(t_2) = \mathcal{L}(t_2 - t_1)\mathcal{L}(t_1)$ does not hold in general. In fact, we can observe an example where the trajectory intersects itself and does not form a closed path in Fig. 3.

If $S_x(0) \neq 0$ or $S_y(0) \neq 0$, $\mathbf{S}(t)$ draws a trajectory in the two- or three-dimensional

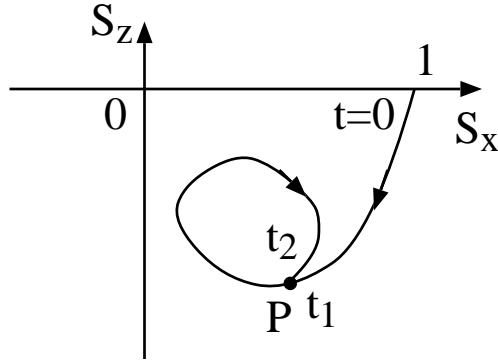


Figure 2: The trajectory of $\mathbf{S}(t)$ whose initial state is given by $\mathbf{S}(0) = (1, 0, 0)$. (We assume $\Delta\omega = 0$.) The horizontal and vertical lines represent S_x and S_z , respectively. They are dimensionless quantities. If $\mathcal{L}(t_2) = \mathcal{L}(t_2 - t_1)\mathcal{L}(t_1)$, the trajectory forms a closed loop. If the trajectory passes a point P at t_1 and reaches P at $t_2 (> t_1)$ again, $\mathbf{S}(t)$ moves along the closed loop for $t \geq t_2$. This is because the evolution of $\mathbf{S}(t)$ is determined by $\mathcal{L}(t - t_2)\mathbf{S}(t_2)$. Actually, $\mathcal{L}(t_2) = \mathcal{L}(t_2 - t_1)\mathcal{L}(t_1)$ does not hold in general and the trajectory does not form the closed path.

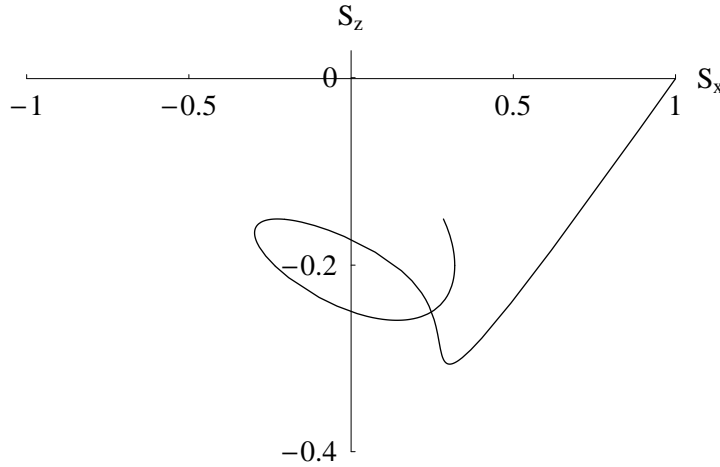


Figure 3: The trajectory of $\mathbf{S}(t)$ ($0 \leq t \leq 6$) whose initial state and temperature are given by $\mathbf{S}(0) = (1, 0, 0)$ and $\beta = 0.5$, respectively. (We assume $\Delta\omega = 0$.) The horizontal and vertical lines represent S_x and S_z , respectively. They are dimensionless quantities. We can observe that the trajectory intersects itself and does not form a closed loop. In the numerical calculation of $L_1(t)$ and $L_4(t)$ defined in Eqs. (28) and (30), the summations of the index n is carried out up to 500.

space. From the above considerations, we understand that this trajectory does not form a closed loop in general.

4 The time-average of the Bloch vector for $\Delta\omega = 0$

In this section, we take the time-average of the Bloch vector for the case where the field is resonant with the atom ($\Delta\omega = 0$). As shown in Fig. 1, the evolution of $\mathbf{S}(t)$ is in complete disorder. To remove the fast frequency oscillation, we consider the time-average of $\mathbf{S}(t)$ as

$$\langle \mathbf{S} \rangle = \lim_{T \rightarrow \infty} \frac{1}{T} \int_0^T dt \mathbf{S}(t). \quad (31)$$

From Eqs. (27), (28), (29) and (30), we obtain

$$\langle \mathbf{S} \rangle = \begin{pmatrix} \langle L_1 \rangle & 0 & 0 \\ 0 & \langle L_1 \rangle & 0 \\ 0 & 0 & \langle L_3 \rangle \end{pmatrix} \mathbf{S}(0) + \begin{pmatrix} 0 \\ 0 \\ \langle L_4 \rangle \end{pmatrix}, \quad (32)$$

$$\begin{aligned} \langle L_1 \rangle &= (1 - e^{-\beta}) \lim_{T \rightarrow \infty} \frac{1}{T} \sum_{n=0}^{\infty} [\sqrt{n+1} \sin(\sqrt{n+1}T) \cos(\sqrt{n}T) \\ &\quad - \sqrt{n} \cos(\sqrt{n+1}T) \sin(\sqrt{n}T)] e^{-n\beta}, \end{aligned} \quad (33)$$

$$\langle L_3 \rangle = \frac{1}{2}(1 - e^{-\beta}) + \frac{e^{2\beta} - 1}{4e^\beta} \lim_{T \rightarrow \infty} \frac{1}{T} \sum_{n=1}^{\infty} \frac{\sin(2\sqrt{n}T)}{\sqrt{n}} e^{-n\beta}, \quad (34)$$

$$\langle L_4 \rangle = -\frac{1}{2}(1 - e^{-\beta}) + \frac{(e^\beta - 1)^2}{4e^\beta} \lim_{T \rightarrow \infty} \frac{1}{T} \sum_{n=1}^{\infty} \frac{\sin(2\sqrt{n}T)}{\sqrt{n}} e^{-n\beta}. \quad (35)$$

Let us take the limit of $T \rightarrow \infty$ in Eqs. (33), (34) and (35). First, we evaluate $\langle L_1 \rangle$. We can obtain the following relation about $\langle L_1 \rangle$ from Eq. (33):

$$-V_1 \leq \langle L_1 \rangle \leq V_1, \quad (36)$$

where

$$V_1 = \frac{e^{2\beta} - 1}{e^\beta} \lim_{T \rightarrow \infty} \frac{1}{T} \sum_{n=0}^{\infty} \sqrt{n} e^{-n\beta} (\geq 0). \quad (37)$$

From Eq. (37), we can derive the following relation:

$$V_1 < \frac{e^{2\beta} - 1}{e^\beta} \lim_{T \rightarrow \infty} \frac{1}{T} \sum_{n=0}^{\infty} n e^{-n\beta}. \quad (38)$$

Because

$$\sum_{n=0}^{\infty} n e^{-n\beta} = \frac{e^\beta}{(e^\beta - 1)^2}, \quad (39)$$

we obtain

$$V_1 < \lim_{T \rightarrow \infty} \frac{1}{T} \frac{e^\beta + 1}{e^\beta - 1}. \quad (40)$$

Thus, if $\beta \neq 0$, $V_1 = 0$ and $\langle L_1 \rangle = 0$. Moreover, we can derive $\langle L_1 \rangle = 0$ for $\beta = 0$ from Eq. (33) in direct. Hence, we obtain $\langle L_1 \rangle = 0 \forall \beta$.

Second, we evaluate $\langle L_3 \rangle$. We can obtain the following relation about $\langle L_3 \rangle$ from Eq. (34):

$$-V_3 \leq \frac{e^{2\beta} - 1}{4e^\beta} \lim_{T \rightarrow \infty} \frac{1}{T} \sum_{n=1}^{\infty} \frac{\sin(2\sqrt{n}T)}{\sqrt{n}} e^{-n\beta} \leq V_3, \quad (41)$$

where

$$V_3 = \frac{e^{2\beta} - 1}{4e^\beta} \lim_{T \rightarrow \infty} \frac{1}{T} \sum_{n=1}^{\infty} \frac{e^{-n\beta}}{\sqrt{n}} (\geq 0). \quad (42)$$

Moreover, we can derive the following relation:

$$V_3 < \frac{e^{2\beta} - 1}{4e^\beta} \lim_{T \rightarrow \infty} \frac{1}{T} \sum_{n=1}^{\infty} e^{-n\beta}. \quad (43)$$

Because $\sum_{n=1}^{\infty} e^{-n\beta} = 1/(e^\beta - 1)$, we obtain

$$V_3 < \lim_{T \rightarrow \infty} \frac{1}{T} \frac{e^\beta + 1}{4e^\beta} = 0. \quad (44)$$

Thus, we obtain

$$\langle L_3 \rangle = \frac{1}{2}(1 - e^{-\beta}). \quad (45)$$

By a similar derivation, we can obtain

$$\langle L_4 \rangle = -\frac{1}{2}(1 - e^{-\beta}). \quad (46)$$

5 The histogram of $S_z(t)$ sampled at intervals of Δt

In this section, we think about the histogram of $\{S_z(n\Delta t) | n = 0, 1, \dots, N\}$ for small Δt and large N . To simplify the discussion, we assume $\Delta\omega = 0$ and $\mathbf{S}(0) = (0, 0, 0)$. The time evolution of $\mathbf{S}(t)$ is described as $\mathbf{S}(t) = (0, 0, L_4(t))$, where $L_4(t)$ is given by Eq. (30).

We investigate the time evolution of $L_4(t)$ by the following way. Fixing β at a certain value and defining a small time interval Δt , we collect $(N+1)$ samples of $L_4(n\Delta t)$ for $n = 0, 1, \dots, N$, where N is large enough. Next, we make a histogram of these $(N+1)$ samples $\{L_4(0), L_4(\Delta t), \dots, L_4(N\Delta t)\}$. We adjust the class interval of bins of the histogram, so that the line graph of the histogram approaches a smooth curve.

This histogram represents an absolute value of a derivative of the inverse function of $L_4(t)$. As shown in Fig. 4, the probability that there is a sample $L_4(n\Delta t)$ in the range of the bin of the histogram $[y, y + \Delta y)$ is proportional to

$$\left| \frac{L_4^{-1}(y + \Delta y) - L_4^{-1}(y)}{\Delta y} \right|, \quad (47)$$

where $t = L_4^{-1}(y)$ is an inverse function of $y = L_4(t)$ and Δy is a class interval of the bin. (Here, we assume $L_4^{-1}(y)$ is not a multi-valued function.) If we take the limit of small Δy ,

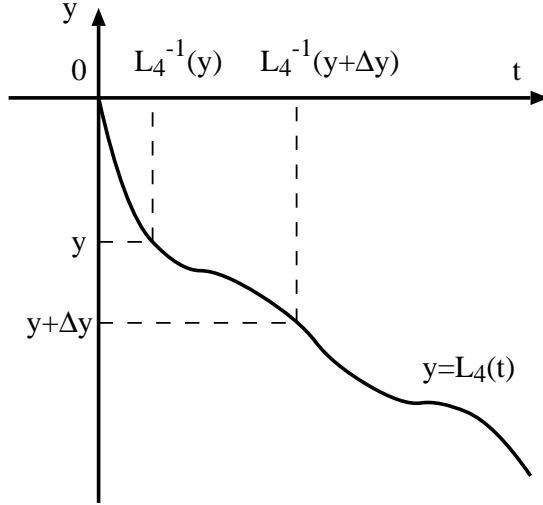


Figure 4: The graph of $y = L_4(t)$. The horizontal and vertical lines represent t and y (or L_4), respectively. t is in units of the time and y (or L_4) is a dimensionless quantity. $t = L_4^{-1}(y)$ is an inverse function of $y = L_4(t)$.

this probability reaches

$$\propto \left| \lim_{\Delta y \rightarrow 0} \frac{L_4^{-1}(y + \Delta y) - L_4^{-1}(y)}{\Delta y} \right| = \left| \frac{d}{dy} L_4^{-1}(y) \right|. \quad (48)$$

If $L_4^{-1}(y)$ is a multi-valued function, the probability is proportional to a summation of $|(d/dy)L_4^{-1}|$ at points whose real parts are equal to y on the Riemann surface.

Let us evaluate the histogram of $L_4(t)$ in the low temperature limit. In the low temperature limit, we can describe $L_4(t)$ as

$$y = \lim_{\beta \rightarrow \infty} L_4(t) = -\frac{1}{2}[1 - \cos(2t)]. \quad (49)$$

Thus, the histogram is proportional to

$$\left| \frac{dt}{dy} \right| = \frac{1}{\sqrt{1 - (2y + 1)^2}} \quad \text{for } -1 \leq y \leq 0. \quad (50)$$

Next, we consider the histogram of $L_4(t)$ for the high temperature. If $\beta \ll 1$, we can expect that $L_4(t)$ varies at random around a mean with a certain variance. Hence, we can approximate the histogram by the probability function of the normal distribution,

$$\frac{1}{\sqrt{2\pi}\sigma} e^{-(y-\mu)^2/(2\sigma^2)}, \quad (51)$$

where μ and σ^2 are a mean and a variance of samples, that is,

$$\mu = \frac{1}{N+1} \sum_{n=0}^N L_4(n\Delta t), \quad (52)$$

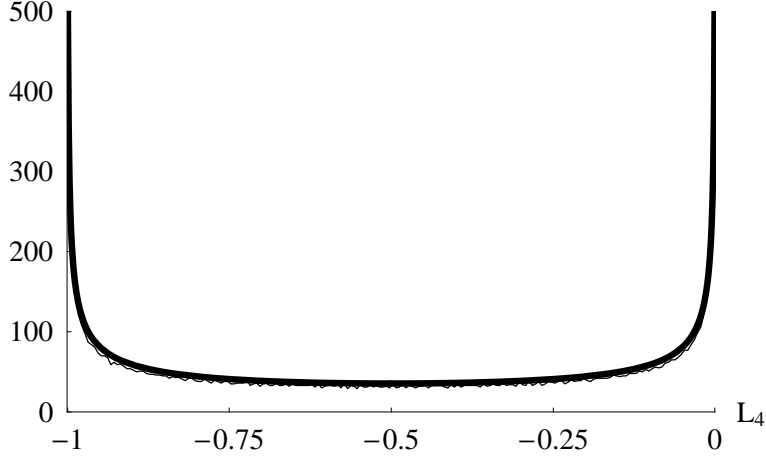


Figure 5: The histogram of $\{L_4(n\Delta t)|n = 0, 1, \dots, 9999\}$ where $\beta = 10$, $\Delta t = 0.05$ and the class interval of each bin is equal to 0.005. The horizontal line represents L_4 that is a dimensionless quantity. The vertical line represents the number of samples in each bin and it is a dimensionless quantity, as well. A thin line graph represents the histogram of samples $\{L_4(n\Delta t)\}$. A thick curve represents the approximate function $a/\sqrt{1 - (2y + 1)^2}$ where $a = 35.5$. In the figure, the thick curve is lying on the thin line graph and we can hardly distinguish between them. In the numerical calculation of $L_4(t)$ defined in Eq. (30), the summation of the index n is carried out up to 1000.

and

$$\sigma^2 = \frac{1}{N + 1} \sum_{n=0}^N [\mu - L_4(n\Delta t)]^2. \quad (53)$$

If $N\Delta t$ is large enough, μ is nearly equal to $\langle L_4 \rangle$. [From Eq. (30), we can show $-1 \leq L_4(t) \leq 0$. Thus, we can expect that $L_4(t)$ varies at random in the range of $[-1, 0]$. However, Eq. (51) is defined on $-\infty < y < \infty$. Here, we neglect this inconsistency.]

In Figs. 5, 6 and 7, we show the histogram of $L_4(t)$ for $\beta = 10$, 1 and 0.01, respectively. In Fig. 5, Eq. (50) fits for the histogram well. In Fig. 7, Eq. (51) fits for the histogram well, too. [In Fig. 7, the shape of the histogram is not symmetrical. A slope of the left side is steeper than a slope of the right side. The author cannot find a physical meaning of this observation.] The histogram of Fig. 6 seems to be an intermediate shape of Figs. 5 and 7.

In Fig. 8, we plot the variance σ^2 of samples against β for $0.01 \leq \beta \leq 10$. For small β , we can approximate plotted points by $\sigma^2(\beta) = c_1\beta^{c_2}$ for $0.01 \leq \beta \leq 0.1$, where $c_1 = 0.0516$ and $c_2 = 2.95$. The author cannot find a reason why the function of $\sigma^2(\beta)$ for small β has such a simple form.

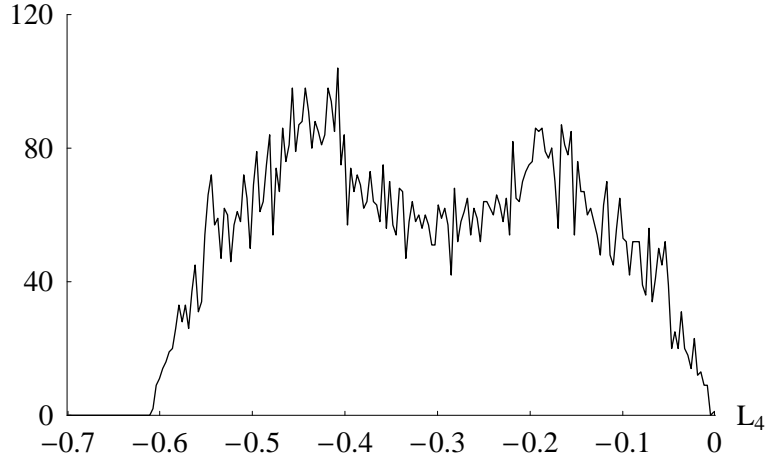


Figure 6: The histogram of $\{L_4(n\Delta t)|n = 0, 1, \dots, 9999\}$ where $\beta = 1$, $\Delta t = 0.05$ and the class interval of each bin is equal to 0.0035. The horizontal line represents L_4 that is a dimensionless quantity. The vertical line represents the number of samples in each bin and it is a dimensionless quantity, as well. In the numerical calculation of $L_4(t)$ defined in Eq. (30), the summation of the index n is carried out up to 1000.

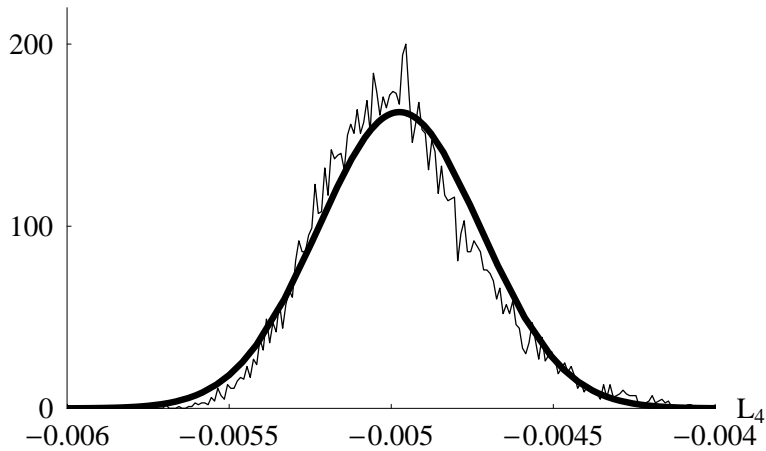


Figure 7: The histogram of $\{L_4(n\Delta t)|n = 0, 1, \dots, 9999\}$ where $\beta = 0.01$, $\Delta t = 0.05$ and the class interval of each bin is equal to 1.0×10^{-5} . The horizontal line represents L_4 that is a dimensionless quantity. The vertical line represents the number of samples in each bin and it is a dimensionless quantity, as well. A thin line graph represents the histogram of samples $\{L_4(n\Delta t)\}$. A thick curve represents the approximate function $[a/(\sqrt{2\pi}\sigma)] \exp[-(y - \mu)^2/(2\sigma^2)]$ where $a = 163$, $\mu = -0.00497$ and $\sigma^2 = 6.31 \times 10^{-8}$. (We note $\langle L_4 \rangle = -0.00498$.) In the numerical calculation of $L_4(t)$ defined in Eq. (30), the summation of the index n is carried out up to 1000.

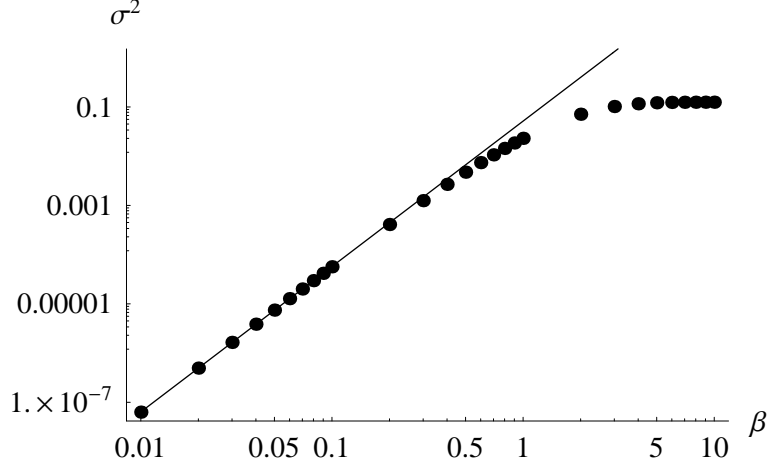


Figure 8: Plots of the variance σ^2 of samples $\{L_4(n\Delta t)\}$ against β for $0.01 \leq \beta \leq 10$. Black circles represent plotted data. For each black circle, ten thousands samples are taken ($n = 0, 1, \dots, 9999$) and we put $\Delta t = 0.05$. The horizontal line represents β that is in units of $(\hbar\omega_0)^{-1}$. The vertical line represents σ^2 that is a dimensionless quantity. In both horizontal and vertical lines, ticks are put in the logarithmic scale. In the range of $0.01 \leq \beta \leq 0.1$, plots can be approximated by $\sigma^2(\beta) = c_1\beta^{c_2}$ where $c_1 = 0.0516$ and $c_2 = 2.95$. This approximate function is shown as a line graph in the figure.

6 The time-average of the Bloch vector for $\Delta\omega \neq 0$

In this section, we evaluate the time-average of the Bloch vector for the non-resonant case ($\Delta\omega \neq 0$). Here, we put $\hbar = 1$ (β is in units of \hbar). We fix g and ω_0 and regard them as constants. Thus, the model has three variables, ω , β and t . From Eqs. (21), (25) and (26), we obtain the following relation:

$$\langle \mathbf{S} \rangle = \begin{pmatrix} \langle L_{\Delta\omega}^{(1)} \rangle & \langle L_{\Delta\omega}^{(2)} \rangle & 0 \\ -\langle L_{\Delta\omega}^{(2)} \rangle & \langle L_{\Delta\omega}^{(1)} \rangle & 0 \\ 0 & 0 & \langle L_{\Delta\omega}^{(3)} \rangle \end{pmatrix} \mathbf{S}(0) + \begin{pmatrix} 0 \\ 0 \\ \langle L_{\Delta\omega}^{(4)} \rangle \end{pmatrix}, \quad (54)$$

where

$$\begin{aligned} \langle L_{\Delta\omega}^{(1)} \rangle &= (1 - e^{-\beta\omega}) \lim_{T \rightarrow \infty} \frac{1}{T} \sum_{n=0}^{\infty} \left[\frac{n+1}{\sqrt{\tilde{D}(n+1)}} \sin(\sqrt{\tilde{D}(n+1)}T) \cos(\sqrt{\tilde{D}(n)}T) \right. \\ &\quad \left. - \frac{n}{\sqrt{\tilde{D}(n)}} \cos(\sqrt{\tilde{D}(n+1)}T) \sin(\sqrt{\tilde{D}(n)}T) \right] e^{-n\beta\omega}, \\ \langle L_{\Delta\omega}^{(2)} \rangle &= -\frac{\Delta\omega}{2} (1 - e^{-\beta\omega}) \lim_{T \rightarrow \infty} \frac{1}{T} \sum_{n=0}^{\infty} \frac{\sin(\sqrt{\tilde{D}(n+1)}T) \sin(\sqrt{\tilde{D}(n)}T)}{\sqrt{\tilde{D}(n+1)\tilde{D}(n)}} e^{-n\beta\omega}, \\ \langle L_{\Delta\omega}^{(3)} \rangle &= (1 - e^{-\beta\omega}) \sum_{n=1}^{\infty} \left[e^{\beta\omega} \frac{(\Delta\omega/2)^2}{\tilde{D}(n)} + \frac{1}{2} (e^{\beta\omega} - 1) \frac{g^2 n}{\tilde{D}(n)} \right] e^{-n\beta\omega} \end{aligned}$$

$$\begin{aligned}
& + \frac{e^{2\beta\omega} - 1}{4e^{\beta\omega}} \lim_{T \rightarrow \infty} \frac{1}{T} \sum_{m=1}^{\infty} \frac{g^2 m}{\tilde{D}(m)} \frac{\sin(2\sqrt{\tilde{D}(m)}T)}{\sqrt{\tilde{D}(m)}} e^{-m\beta\omega}, \\
\langle L_{\Delta\omega}^{(4)} \rangle & = (1 - e^{-\beta\omega}) \sum_{n=1}^{\infty} \left[e^{\beta\omega} \frac{(\Delta\omega/2)^2}{\tilde{D}(n)} + \frac{1}{2}(e^{\beta\omega} + 1) \frac{g^2 n}{\tilde{D}(n)} \right] e^{-n\beta\omega} \\
& + \frac{(e^{\beta\omega} - 1)^2}{4e^{\beta\omega}} \lim_{T \rightarrow \infty} \frac{1}{T} \sum_{m=1}^{\infty} \frac{g^2 m}{\tilde{D}(m)} \frac{\sin(2\sqrt{\tilde{D}(m)}T)}{\sqrt{\tilde{D}(m)}} e^{-m\beta\omega} - 1. \tag{55}
\end{aligned}$$

Using the method shown in Sec. 4, we can take the limit $T \rightarrow \infty$ in Eq. (55) and we obtain

$$\begin{aligned}
\langle L_{\Delta\omega}^{(1)} \rangle & = \langle L_{\Delta\omega}^{(2)} \rangle = 0, \\
\langle L_{\Delta\omega}^{(3)} \rangle & = (1 - e^{-\beta\omega}) \sum_{n=1}^{\infty} \left[e^{\beta\omega} \frac{(\Delta\omega/2)^2}{\tilde{D}(n)} + \frac{1}{2}(e^{\beta\omega} - 1) \frac{g^2 n}{\tilde{D}(n)} \right] e^{-n\beta\omega}, \\
\langle L_{\Delta\omega}^{(4)} \rangle & = (1 - e^{-\beta\omega}) \sum_{n=1}^{\infty} \left[e^{\beta\omega} \frac{(\Delta\omega/2)^2}{\tilde{D}(n)} + \frac{1}{2}(e^{\beta\omega} + 1) \frac{g^2 n}{\tilde{D}(n)} \right] e^{-n\beta\omega} - 1. \tag{56}
\end{aligned}$$

Looking at Eq. (56), we obtain

$$\lim_{\beta \rightarrow 0} \langle L_{\Delta\omega}^{(3)} \rangle = \lim_{\beta \rightarrow 0} \langle L_{\Delta\omega}^{(4)} \rangle = 0, \tag{57}$$

$$\lim_{\beta \rightarrow \infty} \langle L_{\Delta\omega}^{(3)} \rangle = \frac{(\Delta\omega)^2 + 2g^2}{(\Delta\omega)^2 + 4g^2}, \tag{58}$$

and

$$\lim_{\beta \rightarrow \infty} \langle L_{\Delta\omega}^{(4)} \rangle = -\frac{2g^2}{(\Delta\omega)^2 + 4g^2}. \tag{59}$$

The above results imply $\lim_{\beta \rightarrow 0} \langle \mathbf{S} \rangle = \mathbf{0} \forall \mathbf{S}(0)$ and

$$\lim_{\beta \rightarrow \infty} \langle \mathbf{S} \rangle = (0, 0, \frac{[(\Delta\omega)^2 + 2g^2]S_z(0) - 2g^2}{(\Delta\omega)^2 + 4g^2}) \quad \forall \mathbf{S}(0). \tag{60}$$

From Eq. (60), we can say the following: If we start from $\mathbf{S}(0) = \mathbf{0}$ [the complete mixed state $\rho_A(0) = (1/2)\mathbf{I}$] in the low temperature limit, we can expect to obtain a slightly purified state of $\mathbf{S} = (0, 0, -2g^2/[(\Delta\omega)^2 + 4g^2])$ on average after the enough time evolution.

7 Discussions

In this paper, we examine the dynamics of the Bloch vector of the two-level atom in the thermal Jaynes-Cummings model (JCM). In the evolution of the Bloch vector, for example, if $\Delta\omega = 0$, infinite summation of $\cos(\sqrt{n+1}t) \cos(\sqrt{nt})e^{-n\beta}$ and $\cos(2\sqrt{nt})e^{-n\beta}$ for $n = 0, 1, 2, \dots$ appears and this makes it difficult to treat the problem exactly.

In our model, the thermal effects are introduced only in the initial state of the boson field. To discuss the thermodynamics of the JCM strictly, we have to think the grand

partition function of the whole system (the atom and the boson field) and pursue its non-equilibrium time evolution. Although the JCM has been studied by many researchers, understanding about the thermal JCM seems not to be enough.

In this paper, we try to obtain a global property that characterizes the confused behavior of the Bloch vector. We observe the trajectory of the Bloch vector and take its time-average. We take the histogram of the z components of the Bloch vector sampled at intervals of Δt . However, the author wonders whether these results are good global aspects of the trajectory that is in complete disorder.

Recently, entanglement generation during the evolution of JCM has been studied from the viewpoint of the quantum information theory. The thermal JCM may become an important source of entanglement in future.

References

- [1] E.T. Jaynes and F.W. Cummings, ‘Comparison of quantum and semiclassical radiation theories with application to the beam maser’, *Proc. IEEE* **51**, 89–109 (1963).
- [2] B.W. Shore and P.L. Knight, ‘The Jaynes-Cummings model’, *J. Mod. Optics* **40**, 1195–1238 (1993).
- [3] D.F. Walls and G.J. Milburn, *Quantum optics* (Springer-Verlag, Berlin, 1994), Sec. 10.2.
- [4] W.H. Louisell, *Quantum statistical properties of radiation* (John Wiley & Sons, Inc., New York, 1973), Sec. 5.13.
- [5] W.P. Schleich *Quantum optics in phase space* (Wiley-VCH, Berlin, 2001), Chap. 15.
- [6] G. Arroyo-Correa and J.J. Sanchez-Mondragon, ‘The Jaynes-Cummings model thermal revivals’, *Quantum Opt.* **2**, 409–421 (1990).
- [7] S.M. Chumakov, M. Kozirowski and J.J. Sanchez-Mondragon, ‘Analytical approach to the photon statistics in the thermal Jaynes-Cummings model with an initially unexcited atom’, *Phys. Rev. A* **48**, 4594–4597 (1993).
- [8] W.S. Liu and P. Tombesi, ‘Thermal photon distributions in the Jaynes-Cummings model’, *Quantum Opt.* **4**, 229–243 (1992).
- [9] M. Murao and F. Shibata, ‘Dynamics of a dissipative Jaynes-Cummings model’, *J. Phys. Soc. Jpn.* **64**, 2394–2404 (1995).
- [10] C. Uchiyama and F. Shibata, ‘Theory of spin relaxation in a quantum environment: strongly coupled spin-boson system’, *Phys. Lett. A* **267**, 7–17 (2000).
- [11] S. Bose and I. Fuentes-Guridi, P.L.Knight and V. Vedral, ‘Subsystem purity as an enforcer of entanglement’, *Phys. Rev. Lett.* **87**, 050401 (2001); *Phys. Rev. Lett.* **87**, 279901(E) (2001).

- [12] S. Scheel, J. Eisert, P.L. Knight and M.B. Plenio, ‘Hot entanglement in a simple dynamical model’, *J. Mod. Optics* **50**, 881-889 (2003).